Computational Materials Science 129 (2017) 171–177

Contents lists available at ScienceDirect

Computational Materials Science

journal homepage: www.elsevier.com/locate/commatsci

Magnetism and magnetocrystalline anisotropy in vacancy doped and (non)metal adsorbed single-layer $PtSe_2$

Wei Zhang [a,*], Xiao Jiao Song [a], Nan Zhou [a], Hao Li [a], Jie Huang [b]

[a] Physicochemical Group of Department of Criminal Science and Technology, Nanjing Forest Police College, Nanjing 210023, China
[b] Department of Physics, Nanjing Normal University, Nanjing 210023, China

ARTICLE INFO

Article history:
Received 2 October 2016
Received in revised form 15 November 2016
Accepted 5 December 2016

Keywords:
First-principles calculations
Transition-metal dichalcogenide
Adsorption
Magnetocrystalline anisotropy

ABSTRACT

The single-layer (1L) transition-metal dichalcogenides (TMDs) have attracted great attentions over the past years. However, most of previous work focus on the Mo(W) TMDs and the pristine 1L-TMDs are often diamagnetic. Recent experimental progress has sparked renewed interest in Pt(Pd) TMDs. Here, using first-principles calculations, we study the functionalization of the newly synthesized 1L-$PtSe_2$ through adatom adsorption and vacancy defect creation. It is found the 1L-$PtSe_2$ with Pt vacancy (V_{Pt}) has large magnetocrystalline anisotropy energy (30.4 meV/V_{Pt}), which is comparable with that of Ir—Co dimer adsorbed graphene. Except for the magnetism induced by the magnetic Fe(Co) adatom, the metal-free magnetism is introduced by the B(F) adatom, and the 1L-$PtSe_2$ shows stronger adsorption capability to nonmetal atoms (H, B, C, N, F) than that of the 1L-MoS_2(1L-$MoSe_2$). In contrast to the case of 1L-MoS_2(1L-$MoSe_2$), significant reconstructions of surfaces are found for the H, B, C and N adsorbed 1L-$PtSe_2$. Moreover, the semiconducting behaviors and spintronic features are modified: Fe(N) adatom causes $n(p)$-type doping, F adsorbed 1L-$PtSe_2$ becomes bipolar semiconductor.

1. Introduction

Trigged by the successful realization of single-layer (1L) graphite (the well known graphene) [1,2], great attentions had been paid to the two-dimensional (2D) materials because of the peculiar physics brought by them and the potential for applications of next generation nanoscale device [3–5]. The lack of band gap made the graphene had a considerable drawback for the applications such as switching operation in digital logic devices [6,7]. In view of this, the researchers had turned their attention to other kinds of 2D materials called transition metal dichalcogenides (TMDs) [3–5,8]. The common structural formula of TMDs is AB_2, where A are the transition metals (Mo, W, Pt, etc.) and B are the chalcogens (S, Se, Te, etc.). Due to the large intrinsic bandgap of 1.8 eV [3,8–15], the 1L-MoS_2 had emerged as a semiconducting alternative to graphene among these TMDs. However, the electron mobility of 1L-MoS_2 was just up to 10 $cm^2/V/s$ at room temperature [3]. The 1L-MoS_2 based field effect transistors [8] had been reported to have a carrier mobility of 200 $cm^2/V/s$. But the enhanced carrier mobility might be just an overestimation caused by the capacitive coupling between the gates of the devices [9]. Yoon et al. had also pointed out 1L-MoS_2 was not ideal for high-performance semiconductor device applications due to the heavy electron effective mass and the low electron mobility [10]. It is thus necessary to find 2D materials not only with sizable bandgap but also with large carrier mobility.

Recently, a new kind of 1L-TMDs $PtSe_2$ (Fig. 1) was synthesized by the direct selenization of the Pt(1 1 1) substrate [17], which sparked renewed interest in Pt and Pd TMDs [17–27]. Although 1L-$PtSe_2$ had an indirect bandgap of 1.2 eV, its photocatalysis performance was comparable to nitrogen-doped TiO_2 nanoparticles [17]. The work of Zhang et al. showed the 1L-$PtSe_2$ had the largest room temperature mobility (~3000 $cm^2/V/s$) among the 14 kinds of 1L-TMDs [22,23]. Very recently, it was reported experimentally the Raman active modes of $PtSe_2$ showed a clear position and intensity dependence with the film thickness [24]. For the first time, Yao et al. reported the experimental realization of unconventional R-2 Rashba effect in the 1L-$PtSe_2$ [25]. Li et al. found the indirect bandgap transformed to the direct one under uniaxial compressive strain [26]. Considering the simplicity of the production method, the sizable bandgap, the good photocatalytic performance and the ultra high electron mobility, 1L-$PtSe_2$ would be a promising 2D material for the nanoscale applications.

An emerging topic in 2D TMD research is the investigation of magnetism as most of the pristine 2D TMDs are intrinsically diamagnetic [28–30], including the 1L-$PtSe_2$. Hydrogenation has been

* Corresponding author.
E-mail address: zhangw@nfpc.edu.cn (W. Zhang).

http://dx.doi.org/10.1016/j.commatsci.2016.12.008
0927-0256/

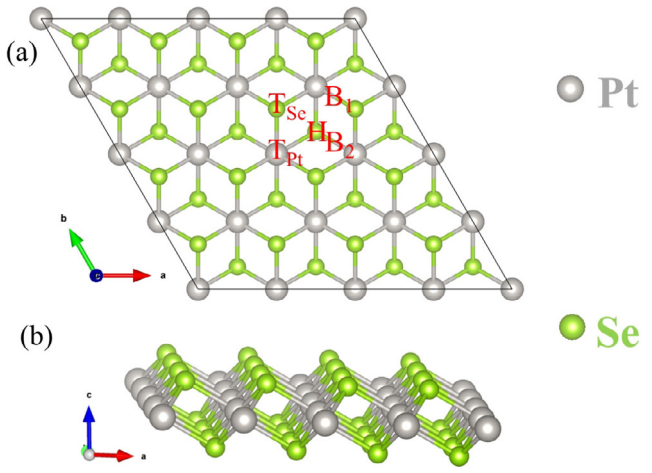

Fig. 1. (a) Topview and (b) sideview of the $4 \times 4 \times 1$ supercell of 1L-$PtSe_2$. All the possible adsorption sites are marked by red. This figure is plotted using VESTA [16]. (For interpretation of the references to color in this figure legend, the reader is referred to the web version of this article.)

proposed in the literature to induce the magnetism of 1L-$PtSe_2$ [27]. We note that the 1L-TMDs often have vacancy (V_X) during the synthesis process [31]. The V_X can also be easily formed by the electron beam [32]. Importantly, it has been noticed in recent years that the V_X played the crucial role in the magnetism of TMDs and graphene. In this context, it is interesting to see whether the V_X is able to induce the magnetism of 1L-$PtSe_2$. As a 2D system, the surface area to volume ratios of nanosheets are always larger than that of the bulk forms, which makes the nanosheets possess higher chemical activity to foreign atoms. Many previous work on 2D materials such as 1L-MoS_2 [33,34] and black phosphorus [35–37] had revealed the magnetic properties and electronic structures could be tuned by surface adsorption, but so far few works focused on the study of adsorption of 5*d* metal based 1L-TMD [38]. It is desirable to known whether the adatom can induce the magnetism and how strong the adsorption ability is for the 5*d* metal based 1L-TMD.

On the other hand, current research interests of the 2D material also focus on the quest for nanoscale information storage devices with large magnetocrystalline anisotropy energy (MAE) [39–42]. Typically, the reduced symmetry and low dimensionality would induce appreciable MAE. The MAE is a fundamentally relativistic effect which originates from the coupling between the spin and orbital degrees of freedom. Thus 5*d* elements which have strong spin-orbit coupling (SOC) are potential candidates for magnetic nanostructures. For example, large MAE had been found in the dimer adsorbed graphene [41,42]. Hence, another question arises: can vacancy doped 1L-$PtSe_2$ or adatom adsorbed 1L-$PtSe_2$ has considerable MAE if they have magnetism?

2. Computational details

All calculations are performed using the projector augmented wave (PAW) method [43], as implemented in the vasp [44,45] code. The exchange-correlation functional is treated by the generalized gradient approximation (GGA) [46]. To describe the electron-ion interaction, the PAW potentials are used, with 10 valence electrons for Pt ($5d^9 6s^1$), 6 for Se ($4s^2 4p^4$). To simulate the adsorption of isolated atom and the vacancy, a $4 \times 4 \times 1$ supercell with 48 atoms is constructed. A larger supercell ($5 \times 5 \times 1$) is tested, the main conclusions remain the same. Convergency tests are performed first, which show the total energies are more sensitive to the plane-wave cutoff energy than that of the *k*-meshes. Thus we use a plane-wave cutoff of 600 eV throughout. For the structural optimizations and density of states (DOS) calculations, a $3 \times 3 \times 1$ and a $7 \times 7 \times 1$ *k*-meshes [47] are adopted respectively. Using these parameters, the energy can converge to less than 0.02 meV/atom. The crystal structures are relaxed until the residual atomic forces are lower than 0.01 eV/Å. To avoid the interactions between adjacent monolayers, a vacuum space of 15 Å in the direction normal to the layers is used. During the calculations of MAE, the SOC is included using the non-collinear mode of vasp. The convergence criteria for total energy is 10^{-7} eV. For comparison, we also study the effect of van der Waals (vdW) interaction in the adsorption calculations using Grimme's DFT+D3 method [48].

3. Results and discussion

3.1. 1L-$PtSe_2$ with V_X

We first study the magnetism of perfect 1L-$PtSe_2$. We consider two types of antiferromagnetic orderings (AFM-I [51] and AFM-II [51–53]) except for the cases of nonmagnetic (NM) and ferromagnetic (FM). The two types of AFM were proposed recently in the explorations of magnetism of perfect 1L-TMDs. It is found the FM states and the AFM states relax to the NM states with equal total energies. These results reflect the expected fact that the t_{2g} orbitals of Pt-5*d* are fully occupied by six electrons (d^6) and the perfect 1L-$PtSe_2$ is NM [27]. Table 1(a) shows the relaxed crystal structure agrees well with previous theoretical calculation [49] and the experiment [50].

Next we study the magnetism of 1L-$PtSe_2$ with V_X. The vacancy formation energy (E_F(V)) is calculated by the formula [54]:

$$E_F(V) = E_{Tot,V} - E_{Tot,Perfect+\mu_V}, \quad (1)$$

where μ_V is the chemical potential of Pt or Se, $E_{Tot,\ Perfect}$ and $E_{Tot,V}$ are the total energies of the perfect supercell and that containing one vacancy respectively. The μ_V depends on the growth condition. In Se poor condition, the upper bound of μ_{Pt} is the energy of Pt in the bulk phase (fcc Pt, $\mu_{Pt} = \frac{1}{4}E_{Pt_{fcc}}$), which results in the lower limit on Se: $\mu_{Se} = \frac{1}{2}(E_{Tot,f.u.} - \mu_{Pt})$. $E_{Tot,f.u.}$ is the energy of formula unit of perfect $PtSe_2$, i.e., $E_{Tot,f.u.} = \frac{1}{16}E_{Tot,Perfect}$. In Se rich condition, the upper bound of μ_{Se} is the energy of Se in the bulk phase (hexagonal Se, $\mu_{Se} = \frac{1}{3}E_{Sehex}$), which leads to the lower limit on μ_{Pt} : $\mu_{Pt} = E_{Tot,f.u.} - 2\mu_{Se}$. As shown in Table 1(b), the calculated $E_F(V_{Se})$ agrees well with previous work [32,55] and the $E_F(V_{Se})$ is lower than the $E_F(V_S)$ of 1L-MoS_2 [32]. The $E_F(V_{Pt})$ is larger the $E_F(V_{Se})$, indicating the V_{Se} is more prone to form than the V_{Pt}.

Then we calculate the total energies differences between the spin-polarized (SP) and the spin-unpolarized (NSP) states for the vacancy doped 1L-$PtSe_2$. It is found the initial SP state converges to the NSP state for the case of V_{Se}, indicating the defect system is NM. However, for the case of V_{Pt}, the total energy of the SP state is 6.5 meV/f.u. lower than the NSP state and the magnetic moment is 4 μB/V_{Pt}, which shows the 1L-$PtSe_2$ with V_{Pt} is magnetic. From the spin density of V_{Pt} (not shown), we find the magnetic moments mainly distribute at the Se(Pt) atoms around(far away) the V_{Pt}, and the distribution shapes reflect the characters of Se *p* orbitals and Pt $d_{x^2-y^2}$ orbitals. We also calculate the MAE for the case of V_{Pt}. The MAE is defined as MAE = $E_x - E_z$ [56], where E_x and E_z denote the total energies of self-consistent calculations in the *x* and *z* magnetization directions, respectively. Interestingly, the calculated MAE shows considerable value of −30.4 meV/V_{Pt}: first, the negative value of MAE indicates the easy axis of V_{Pt} lies in the direction parallel to the $PtSe_2$ layer; second, the MAE of V_{Pt} is comparable with that of Ir—Co dimer adsorbed graphene with single vacancy [42]; third, the MAE just satisfies the request for

Table 1
(a) Lattice constants (a_0(b_0), Å), bond lengths (b_{Pt-Se} and b_{Se-Se}, Å), bond angles ($\theta_{Se-Pt-Se}$, degree) of perfect 1L-$PtSe_2$. The theoretical [49] (The.) data and the experimental [50] (Exp.) data are provided for comparison. (b) Formation energy (E_F, eV) of V_{Se} and V_{Pt}. (c) Structural information of 1L-MoS_2 and 1L-$MoSe_2$. The $b_{S(Se)-S(Se)}$ denotes the bond length of S—S or Se—Se.

(a)	a_0	b_{Pt-Se}	b_{Se-Se}	$\theta_{Se-Pt-Se}$
Cal.	3.75	2.53	3.40	95.67
Exp.[a]	3.73	2.51	3.35	96.13
The.[b]	3.75	2.53	3.40	95.63
(b)		$E_F(V_{Se})$		$E_F(V_{Pt})$
Se poor		1.24		3
Se rich		1.83		4.19
Se rich[c]		1.81		
		1.82[d]		
(c)	a_0	$b_{Mo-S(Se)}$	$b_{S(Se)-S(Se)}$	$\theta_{S(Se)-Mo-S(Se)}$
MoS_2[b]	3.18	2.41	3.13	80.8
$MoSe_2$[b]	3.32	2.54	3.34	82.18

[a] Ref. [50].
[b] Ref. [49].
[c] Calculated using 5 × 5 × 1 supercell.
[d] Refs. [32,55], calculated using 5 × 5 × 1 supercell.

practical applications of magnetic nanostructure at room temperature [42]. It should be pointed out that although the V_{Pt} has higher E_F than V_{Se}, the V_{Pt} should be created under certain growth conditions. Besides, if the magnetic property of V_{Pt} is promising for applications, other methods such as ion irradiation [32] can be considered to create the V_{Pt} in 1L-$PtSe_2$.

3.2. Adatoms adsorptions

Now, let's turn to the study of adatoms adsorptions on 1L-$PtSe_2$. There are five possible high-symmetry sites (Fig. 1) for the adatoms: the top site (T_{Pt}) above the Pt atom, the top site (T_{Se}) above the Se atom, the hollow site (H) at the center of the buckled hexagon, the bridge site ($B_{1(2)}$) at the midpoint of the Pt—Se bond. Table 2 shows the most favorable adsorption sites for all the adatoms. The corresponding adsorption structures for all the adatoms are shown in Fig. 2.

3.2.1. Adsorption structures and adsorption energies

For the nonmetallic adatoms, the H and N prefer to adsorb at the T_{Pt} site. The B and C favor to occupy the B_1 site. The F adatom prefers the H site. For the O adatom, it prefers to adsorb at both the H and the B sites, and the initial H and B sites relax to the same T_{Se} site. Although these nonmetallic adatoms have different stable adsorption sites, most of them become embedded ("E") into the upper Se atoms after full relaxation. The H, C and N look like to substitute the adjacent native Se atom and strong bond with nearest Pt atoms. For the B adatom, it looks like to substitute the adjacent native Pt atom and the Pt atom is pushed to the lower layer. This grievous phenomenon is not found in $MoSe_2$ [57] and MoS_2 [33]. Note that the lattice constant of 1L-$PtSe_2$ is about 0.5(0.4) Å larger than that of the 1L-MoS_2($MoSe_2$) (Table 1(c)). The bond lengths of 1L-$PtSe_2$ are also larger than (or comparable with) that of the 1L-MoS_2($MoSe_2$). In other words, the 1L-$PtSe_2$ has more adsorption space for the nonmetallic adatoms. Besides, above results suggest the Pt—Se covalent bond should be softer than the Mo—Se(S) covalent bond. The significant reconstruction of surface is also reflected from the E_{ads}. Previous work [33,57] indicated that the E_{ads} of H, B, C, N, O and F adsorbed 1L-$MoSe_2$(MoS_2) are −0.02(−0.6), −2.82(−3.01), −2.6(−2.47), −0.71(−1.38), −3.16 (−3.88) and −2.1(−1.79) eV, respectively. Comparing the E_{ads} between 1L-$PtSe_2$ and 1L-$MoSe_2$(1L-MoS_2), the interactions between 1L-$PtSe_2$ and these nonmetal atoms are stronger than that of the 1L-$MoSe_2$(1L-MoS_2) except for the case of O adsorbed 1L-MoS_2. For the transition metal adatoms (Fe, Co, Ni), we can see from Table 2 that they all prefer to adsorb at the T_{Pt} sites, which is the same to the case of transition metal (Fe, Co, Ni) adsorbed 1L-MoS_2 [58]. For the noble metal adatoms (Ag, Pt, Au), the Ag and Au favor to occupy the H sites while the Pt favor to occupy the T_{Pt} site. Besides, although Pt and Au adatoms favor to occupy different sites, they both have the meta stable sites (B_1 and B_2). The initial B_1 and B_2 sites relax to the T_{Pt} and H sites, respectively.

Table 2
The most favorable adsorption site, adsorption energy (E_{ads}, eV), the adsorption height (h, Å), the magnetic moments of the whole system (M_{tot}, μB) and adatoms (M_{ads}, μB), the charge transfer (ΔQ, e^-) between adatom and $PtSe_2$ monolayer, the magnetic energy (ΔE_M, meV). h is the vertical distance from adatom to the uppermost Se atoms. "X → XX" indicates the most favorable adsorption site X relaxes to the final XX site. "X(←XX)" indicates the most favorable adsorption site is the X site, and the initial adsorption site XX relaxes to the X site.

Adatom	Site	E_{ads}	h	ΔQ	M_{tot}	M_{ads}	ΔE_M
H	T_{Pt} → E	−1.32	−0.41	−0.01	–	–	–
B	B_1 → E	−5.1	−0.86	−0.69	1	0	43.75
C	B_1 → E	−3.62	−0.24	0.57	–	–	–
N	T_{Pt} → E	−2.19	0.14	0.04	–	–	–
O	H(B) → T_{Se}	−3.59	1.56	0.81	–	–	–
F	H	−2.61	1.49	0.59	1	0.09	53.07
Fe	T_{Pt}	−2.6	1.15	−0.6	2.54	2.68	893.75
Co	T_{Pt}	−2.98	1.02	−0.41	1	1.32	250.65
Ni	T_{Pt}	−3.05	1.03	−0.29	–	–	–
Ag	H	−1.02	1.77	−0.26	–	–	–
Pt	T_{Pt}(←B_1)	−3.12	1.33	0.08	–	–	–
Au	H(←B_2)	−1.28	1.74	0.03	–	–	–

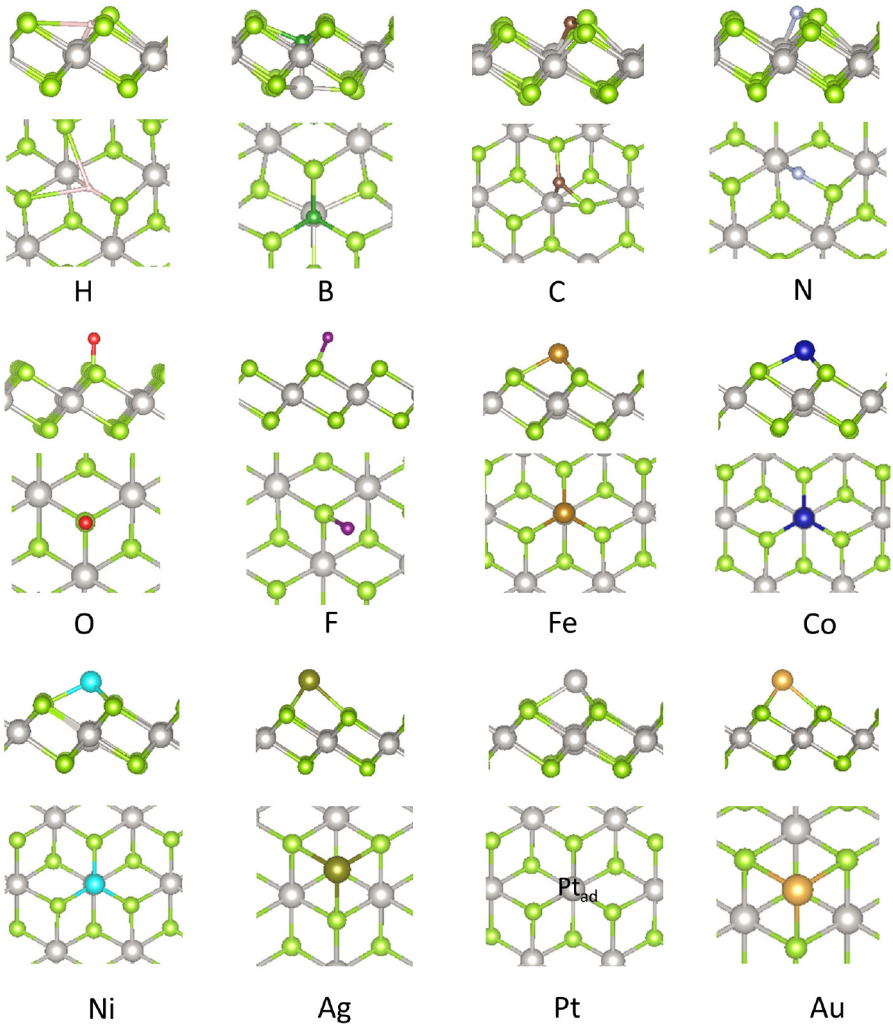

Fig. 2. Sideview (first row) and topview (second row) of the adsorption structures. For clarity the Pt adatom is marked by Pt_{ad}.

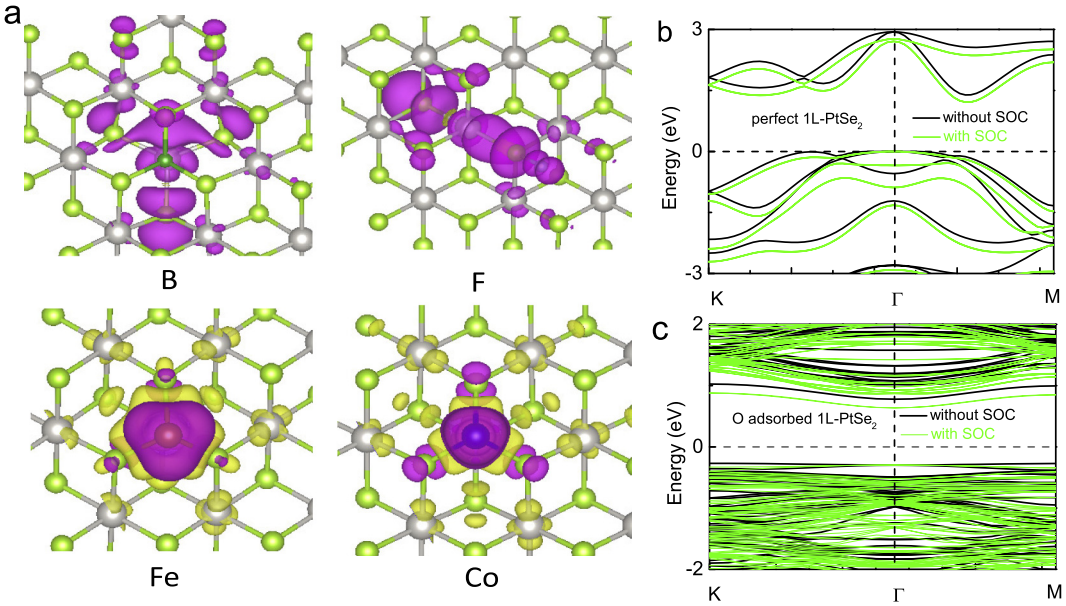

Fig. 3. (a) Spin density of B, F, Fe and Co adsorbed 1L-$PtSe_2$. The violet (yellow) isosurfaces correspond to the positive (negative) spin density. The isosurface value is 0.001 e^-/Bohr^3. (b) Band structure of perfect 1L-$PtSe_2$. Note that the local VBM (between Γ and K) is about 9 meV smaller than the Γ point. The VBM is set as the Fermi level in this subgraph. (c) Band structure of O adsorbed 1L-$PtSe_2$. (For interpretation of the references to color in this figure legend, the reader is referred to the web version of this article.)

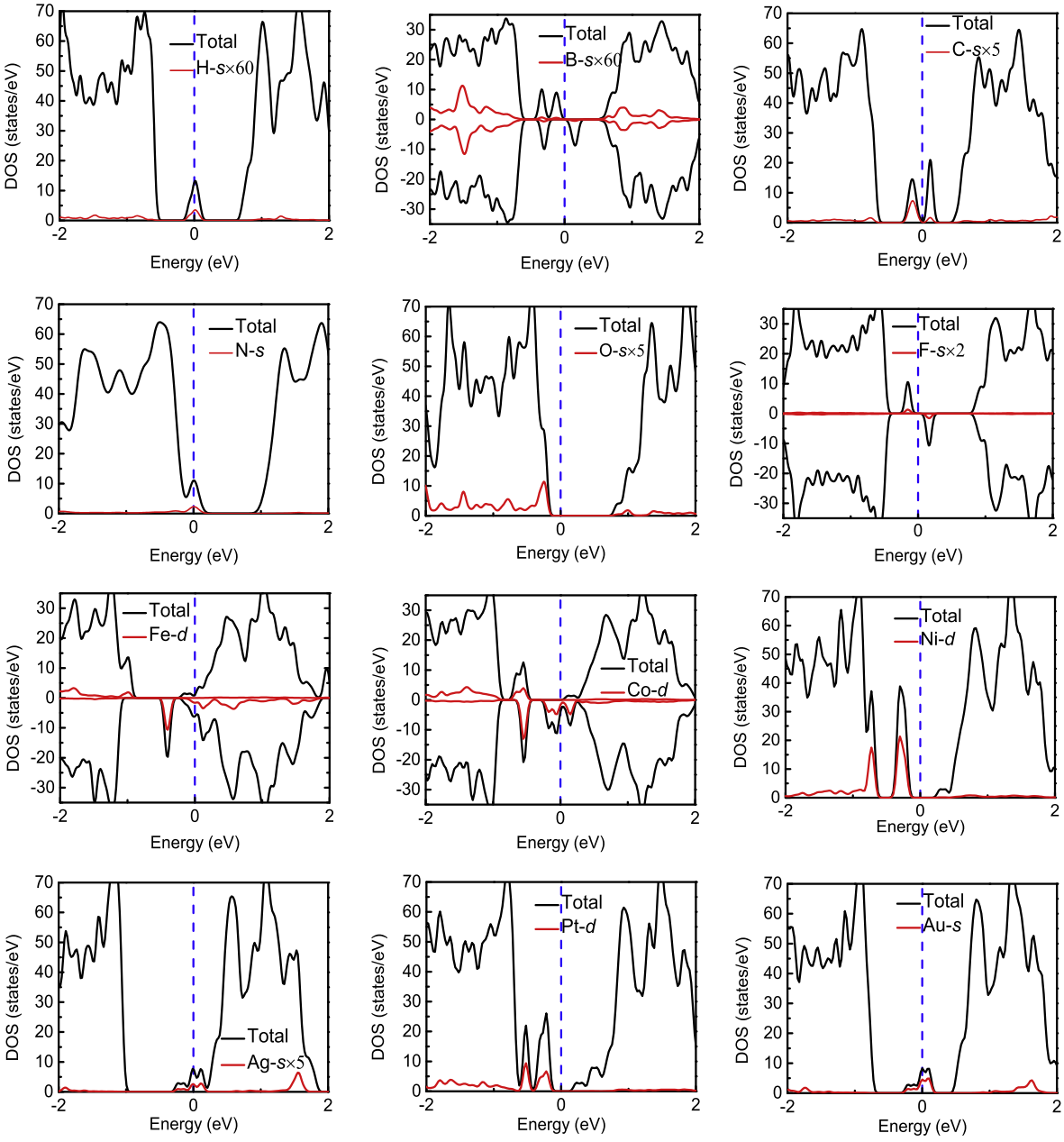

Fig. 4. Total (black) and partial (red) DOS of adatoms decorated 1L-$PtSe_2$. For convenience, some of the partial DOS are magnified. (For interpretation of the references to color in this figure legend, the reader is referred to the web version of this article.)

3.2.2. Charge transfer and magnetic properties

The charge transfers (ΔQ) between adatom and 1L-$PtSe_2$ are calculated by Bader charge analysis. The negative value means the adatom denotes electrons to the 1L-$PtSe_2$. The positive value implies the excess electrons in the adatom, i.e., the adatoms gain electrons from the 1L-$PtSe_2$. It can be seen from Table 2 that there is an obvious electron transfer between the adatom and the 1L-$PtSe_2$ except for the case of H adatom. In the same period, the electronegativity increases from H to N, but the ΔQ does not show too much obvious regularity due to the significant reconstructions of surfaces. F has higher electronegativity than O. However, the ΔQ of F is smaller than that of the O, which is associated to the larger bond length between F and the bonding Se atom. The bond length of F—Se is 1.92 Å while the bond length of O—Se is 1.67 Å. The clear trend of ΔQ can be seen from the transition metal (Fe, Co, Ni) adsorbed systems, where the increasing ΔQ (negative value) is consistent with the increasing electronegativity from Fe to Ni. Among the three noble metal adatoms (Ag, Pt, Au), the electronegativity of Ag is 1.93 according to the Pauling scale, which is obviously lower than other two adatoms (Pt2.28, Au2.54). Thus the Ag adatom denotes electrons to the 1L-$PtSe_2$ whereas the Pt and Au adatoms obtain electrons from the substrate. Then we study the magnetic behavior of the adsorbed system. As expected, the magnetic adatoms (Fe, Co) can induce the magnetism for the decorated 1L-$PtSe_2$. The magnetic moments of the whole systems (M_{tot}) are 2.54 and 1 μB respectively. Comparing with the magnetic moments from *d* electrons of transitional-metal atoms, the magnetism introduced by the nonmetal elements is of particular interest. This is because it was reported that the magnetism based on the *sp* states of nonmetal elements had stronger long-range exchange coupling interactions and no clustering of magnetic ions [59,60]. As shown in Table 2, the B and F adatoms can introduce the

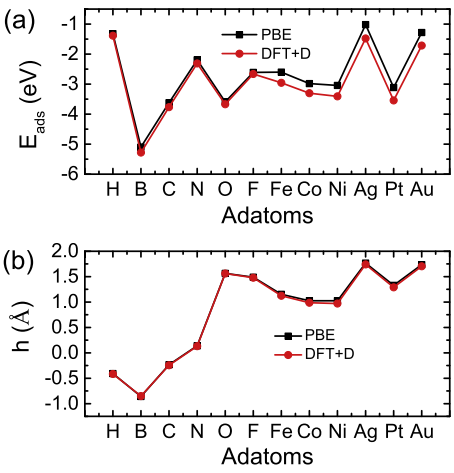

Fig. 5. The comparisons between the PBE and DFT+D methods. (a) Adsorption energy. (b) Adsorption height.

magnetism. The magnetic energy (ΔE_M), which is calculated as $\Delta E_M = E_{MAG} - E_{NM}$ for the decorated 1L-$PtSe_2$, is an important index for the magnetic system. It can be seen from Table 2 that the obtained smallest ΔE_M is 43.75 meV, indicating the magnetism will not be concealed by the thermal fluctuation of the surroundings. Table 2 also clearly shows the difference of magnetism between the transition metal adsorbed systems and the nonmetal adsorbed systems. The M_{tot}s of Fe and Co adsorbed systems mainly come from the adatoms while the B and F adatoms contribute very little to the M_{tot}. We can see more clearly about the difference mentioned above from the spin density shown in Fig. 3(a). Concerning the MAE, we find that only the Co adsorbed 1L-$PtSe_2$ has the MAE of about 5 meV. For other magnetic systems, their MAE nearly equals to zero.

3.2.3. Electronic structures

Finally, let's turn to discuss the electronic structures of adatoms decorated 1L-$PtSe_2$. Before discussion, we briefly review the electronic properties of perfect 1L-$PtSe_2$. As shown in Fig. 3(b), although the calculated theoretical bandgap without including SOC is a little larger than the experimental value, the experimentally observed indirect bandgap character is reproduced. The conduction band minimum (CBM) lies between M and Γ point while the valence band maximum (VBM) locates at the Γ point. The inclusion of SOC makes the degenerate bands at the VBM split into the non-degenerate ones, but the indirect bandgap character is not changed. The effect of SOC on the electronic properties of adatoms decorated 1L-$PtSe_2$ are also considered. We find the band structures of decorated 1L-$PtSe_2$ do not have too much obvious change after considering SOC. Taking O adsorbed 1L-$PtSe_2$ as an example (Fig. 3(c)), we can see the main electronic properties of O adsorbed 1L-$PtSe_2$ are maintained. Therefore in what follows we provide the results without including SOC.

Fig. 4 shows the total and partial DOS of adatoms decorated 1L-$PtSe_2$. It can be seen that all the nonmetal atoms decorated 1L-$PtSe_2$ can maintain the semiconductor character except the H and N atoms. Compared to the band gap of perfect 1L-$PtSe_2$, the band gaps of decorated 1L-$PtSe_2$ are lower. The H adsorption brings the defect state in the middle of the gap. However, the H-*s* orbital nearly has no contribution to the defect state. The defect state is mainly consisted by the *d* orbital of the Pt atom around the H adatom and the *p* orbital of the Se atom which locates at the down Se plane. The B adsorption introduces several defect states in the gap. The DOSs of the up spin and down spin are not symmetrical, which clearly points to the magnetism of B decorated system. Similar to the case of H, the B-*s* orbital itself nearly has no contribution to the nonsymmetric gap states, which also can be seen from the spin density shown in Fig. 3(a). The B-*s* orbitals which have considerable contributions to the total DOS are deep in the valence (conduction) bands. As mentioned in the previous section, the B adatom results in significant reconstruction of the surface, which is quite different from the case of B adsorbed 1L-MoS_2. Interestingly, the total DOSs of B adsorbed 1L-$PtSe_2$ and 1L-MoS_2 are very similar to each other [33]. The C adsorption introduces two defect states in the gap. One locates below the Fermi level and the other locates above the Fermi level. For the N adatom, it introduces a noticeable peak on the top region of VB, moving the Fermi level downward. Thus, the N adatom acts as a *p*-type dopant for the 1L-$PtSe_2$. The O adatom induces several small peaks in the valence bands. It is expected the O adatom should has negligible effect on the electronic properties of 1L-$PtSe_2$. The F adatom introduces a characteristic local spin split state in the gap. Particularly, near the Fermi level, the unoccupied and occupied states belong to different spins, which indicates a bipolar magnetic semiconducting feature [61]. The 3*d* transition metal adatoms (Fe, Co, Ni) also bring the defect states in the gap. Different from the case of nonmetallic adatoms, these defect states are mainly consisted by the adatoms themselves. For the Fe adsorbed system, the main defect states locate below the CBM and the Fermi level moves into the CB, indicating the Fe adatom acts as a *n*-type dopant. For the Ni adsorbed case, the defect states also contribute to the VBM. The Fermi level shifts to the middle of the gap. For the Co adsorption, the Fermi level is occupied by the Co-*d* states. Thus the Co decorated 1L-$PtSe_2$ has certain metallicity. For the noble metal adatoms, they do not introduce magnetism. Except for the Pt adsorption, the Ag and Au adsorbed systems exhibit metallic characters. We have also checked the results using DFT+D method. It is found both the PBE method and the DFT+D method give consistent results about the most favorable adsorption sites. Fig. 5 depicts the comparison between the PBE results and the DFT+D results. We can clearly see the vdW interactions have negligible influences on the nonmetal adsorptions. Although there are small differences for the E_{ads} of the metal adatoms, both the PBE method and the DFT+D method give the same trend about the change of E_{ads}.

4. Conclusions

In summary, using first-principles calculations, we have studied the functionalization of the newly synthesized 1L-$PtSe_2$ by vacancy defect creation and adatom adsorption. We find the 1L-$PtSe_2$ with V_{Pt} has large magnetocrystalline anisotropy energy (30.4 meV/V_{Pt}), which is comparable with that of Ir—Co dimer adsorbed graphene. Comparing with the case of 1L-MoS_2(1L-$MoSe_2$), the 1L-$PtSe_2$ shows stronger adsorption capability to nonmetal atoms (H, B, C, N, F), and the metal-free magnetism is introduced by the B and F adatoms. In contrast to the case of 1L-MoS_2(1L-$MoSe_2$), the H, B, C and N adatoms decorated systems show significant reconstructions of surfaces, which can be attributed to the relatively softer covalent bonding of 1L-$PtSe_2$. Besides, it is found the adatoms adsorptions can effectively modify the spintronic features and semiconducting behaviors: Fe(N) adatom causes *n*(*p*)-type doping, F adsorbed 1L-$PtSe_2$ becomes bipolar semiconductor. These results would provide insight for the potential applications of 1L-$PtSe_2$ in nanoelectronics.

Acknowledgements

Wei Zhang would like to thank Dr. Weixiao Ji and Xiaohui Wang for their help in our research. This work is supported by the Natural Science Foundation of Jiangsu Province (Grant No: BK20161055)

and the Basic Research Project of Central University (Grant Nos: LGYB201610, LGYB201612, LGYB201609). First-principles calculations are performed at the Shanghai Supercomputer Center. Part of the supercomputer time is provided by the HPC Center of Department of Physics at the Nanjing Normal University.

References

[1] K.S. Novoselov, A.K. Geim, S.V. Morozov, D. Jiang, Y. Zhang, S.V. Dubonos, I.V. Grigorieva, A.A. Firsov, Science 306 (2004) 666.
[2] K.S. Novoselov, A.K. Geim, S.V. Morozov, D. Jiang, M.I. Katsnelson, I.V. Grigorieva, S.V. Dubonos, A.A. Firsov, Nature (London) 438 (2005) 197.
[3] K.S. Novoselov, D. Jiang, T.J. Booth, W. Khotkevich, S.V. Morozov, A.K. Geim, Proc. Natl. Acad. Sci. 102 (2005) 10451.
[4] Q.H. Wang, K. Kalantar-Zadeh, A. Kis, J.N. Coleman, M.S. Strano, Nat. Nanotechnol. 7 (2012) 699.
[5] T. Heine, Acc. Chem. Res. 48 (2015) 65.
[6] F. Schwierz, Nat. Nanotechnol. 5 (2010) 487.
[7] Y. Wu, Y.M. Lin, A.A. Bol, A. Jenkins, F. Xia, D.B. Farmer, Y. Zhu, P. Avouris, Nature (London) 472 (2011) 74.
[8] B. Radisavljevic, A. Radenovic, J. Brivio, V. Giacometti, A. Kis, Nat. Nanotechnol. 6 (2011) 147.
[9] M.S. Fuhrer, J. Hone, Nat. Nanotechnol. 8 (2013) 146.
[10] Y. Yoon, K. Ganapathi, S. Salahuddin, Nano Lett. 11 (2011) 3768.
[11] H.L. Zheng, B.S. Yang, D.D. Wang, R.L. Han, X.B. Du, Y. Yan, Appl. Phys. Lett. 104 (2014) 132403.
[12] P. Tao, H.H. Guo, T. Yang, Z.D. Zhang, J. Appl. Phys. 115 (2014) 054305.
[13] E. Scalise, M. Houssa, G. Pourtois, V. Afanasev, A. Stesmans, Nano Res. 5 (2012) 43.
[14] P. Johari, V.B. Shenoy, ACS Nano 6 (2012) 5449.
[15] T.S. Li, Phys. Rev. B 85 (2012) 235407.
[16] K. Momma, F. Izumi, J. Appl. Crystallogr. 41 (2008) 653.
[17] Y.L. Wang, L.F. Li, W. Yao, S.R. Song, J.T. Sun, J.B. Pan, X. Ren, C. Li, E. Okunishi, Y. Q. Wang, E.Y. Wang, Y. Shao, Y.Y. Zhang, H.T. Yang, E.F. Schwier, H. Iwasawa, K. Shimada, M. Taniguchi, Z.H. Cheng, S.Y. Zhou, S.X. Du, S.J. Pennycook, S.T. Pantelides, H.J. Gao, Nano Lett. 15 (2015) 4013.
[18] P. Miro, M. Ghorbani-Asl, T. Heine, Angew. Chem. 53 (2014) 3015.
[19] J. Sun, H. Shi, T. Siegrist, D.J. Singh, Appl. Phys. Lett. 107 (2015) 153902.
[20] Y. Wang, Y. Li, Z. Chen, J. Mater. Chem. C 3 (2015) 9603.
[21] Y.D. Zhao, J.S. Qiao, P. Yu, Z.X. Hu, Z.Y. Lin, S.P. Lau, Z. Liu, W. Ji, Y. Chai, Adv. Mater. 28 (2016) 2399.
[22] W.X. Zhang, Z.S. Huang, W.L. Zhang, Y.R. Li, Nano Res. 7 (2014) 1731.
[23] Z.S. Huang, W.X. Zhang, W.L. Zhang, Y.R. Li, Available from: <1505.05698>.
[24] M. O'Brien, N. McEvoy, C. Motta, J.Y. Zheng, N.C. Berner, J. Kotakoski, K. Elibol, T.J. Pennycook, J.C. Meyer, C. Yim, M. Abid, T. Hallam, J.F. Donegan, S. Sanvito, G.S. Duesberg, 2D Mater. 3 (2016) 2053.
[25] W. Yao, E.Y. Wang, H.Q. Huang, K. Deng, M.Z. Yan, K.N. Zhang, T.C. Okuda, L.F. Li, Y.L. Wang, H.J. Gao, C.X. Liu, W.H. Duan, S.Y. Zhou, Available from: <1603. 02140>.
[26] P.F. Li, L. Li, X.C. Zeng, J. Mater. Chem. C 4 (2016) 3106.
[27] P. Manchanda, A. Enders, D.J. Sellmyer, R. Skomski, Phys. Rev. B 94 (2016) 104426.
[28] A. Kuc, N. Zibouche, T. Heine, Phys. Rev. B 83 (2011) 245213.
[29] Z.Y. Zhu, Y.C. Cheng, U. Schwingenschlogl, Phys. Rev. B 84 (2011) 153402.
[30] C. Ataca, H. Sahin, S. Ciraci, J. Phys. Chem. C 116 (2012) 8983.
[31] W. Zhou, X.L. Zou, S. Najmaei, Z. Liu, Y.M. Shi, J. Kong, J. Lou, P.M. Ajayan, B.I. Yakobson, J.C. Idrobo, Nano Lett. 13 (2013) 2615.
[32] H. Komsa, J. Kotakoski, S. Kurasch, O. Lehtinen, U. Kaiser, A.V. Krasheninnikov, Phys. Rev. Lett. 109 (2012) 035503.
[33] J.G. He, K.C. Wu, R.J. Sa, Q.H. Li, Y.Q. Wei, Appl. Phys. Lett. 96 (2010) 082504.
[34] J.W. Chang, S. Larentis, E. Tutuc, L.F. Register, S.K. Banerjee, Appl. Phys. Lett. 104 (2014) 141603.
[35] Y. Ding, Y.L. Wang, J. Phys. Chem. C 119 (2015) 10610.
[36] T. Hu, J.S. Hong, J. Phys. Chem. C 119 (2015) 8199.
[37] R.Q. Zhang, B. Li, J.L. Yang, J. Phys. Chem. C 119 (2015) 2871.
[38] X.O. Zhang, Q.F. Li, J. Appl. Phys. 118 (2015) 064306.
[39] R. Wiesendanger, Rev. Mod. Phys. 81 (2009) 1495.
[40] D. Sellmyer, R. Skomski, Advanced Magnetic Nanostructures, Springer, New York, 2006.
[41] Y. Zhang, Z. Wang, J.X. Cao, J. Mater. Chem. C 2 (2014) 8817.
[42] J. Hu, R.Q. Wu, Nano Lett. 14 (2014) 1853.
[43] P.E. Blöchl, Phys. Rev. B 50 (1994) 17953.
[44] G. Kresse, J. Furthmüller, Phys. Rev. B 54 (1996) 11169.
[45] G. Kresse, D. Joubert, Phys. Rev. B 59 (1999) 1758.
[46] J.P. Perdew, K. Burke, M. Ernzerhof, Phys. Rev. Lett. 78 (1997) 1396.
[47] H.J. Monkhorst, J.D. Pack, Phys. Rev. B 13 (1976) 5188.
[48] S. Grimme, J. Antony, S. Ehrlich, S. Krieg, J. Chem. Phys. 132 (2010) 154104.
[49] H.L. Zhuang, R.G. Hennig, J. Phys. Chem. C 117 (2013) 20440.
[50] S. Furuseth, K. Selte, A. Kjekshus, Acta. Chem. Scand. 19 (1965) 257.
[51] P. Manchanda, V. Sharma, H.B. Yu, D.J. Sellmyer, R. Skomski, Appl. Phys. Lett. 107 (2015) 032402.
[52] Y.G. Zhou, Z.G. Wang, P. Yang, X.T. Zu, L. Yang, X. Sun, F. Gao, ACS Nano 6 (2012) 9727.
[53] Y. Xu, X.F. Liu, W.L. Guo, Nanoscale 6 (2014) 12929.
[54] C. Freysoldt, B. Grabowski, T. Hickel, J. Neugebauer, G. Kresse, A. Janotti, C.G. VandeWalle, Rev. Mod. Phys. 86 (2014) 253.
[55] Note that in Ref.32 Komsa *et al.* use the total energy of isolated chalcogen atom as the chemical potential (private communication). In order to avoid misunderstanding and to compare the $E_F(V_{Se})$ directly in Se rich condition, we use the energy of Se in the bulk phase and provide the converted $E_F(V_{Se})$ basing on the original data of Komsa *et al.*.
[56] D.S. Wang, R.Q. Wu, A.J. Freeman, Phys. Rev. B 47 (1993) 14932.
[57] Y.D. Ma, Y. Dai, M. Guo, C.W. Niu, J.B. Lu, B.B. Huang, Phys. Chem. Chem. Phys. 13 (2011) 15546.
[58] C. Ataca, S. Ciraci, J. Phys. Chem. C 115 (2011) 13303.
[59] O.V. Yazyev, L. Helm, Phys. Rev. B 75 (2007) 125408.
[60] J.J. Attema, G.A. de Wijs, G.R. Blake, R.A. de Groot, J. Am. Chem. Soc. 127 (2005) 16325.
[61] X.X. Li, X.J. Wu, Z.Y. Li, J.L. Yang, J.G. Hou, Nanoscale 4 (2012) 5680.